

Interplay Between the Dissolved Mn²⁺ and Solid Electrolyte Interphases of Graphite Anode

Cong Zhong, Siheng Niu, Yixin Li, Suting Weng, Jiacheng Zhu, Zhaoxiang Wang, Lifan Wang, Ting Feng, Xiaoqi Han, Yejing Li,* Shaofei Wang,* Hong Li, Chun Zhan,* and Xuefeng Wang*

Transition metal (TM) dissolution and crosstalk are one of the main degradation mechanisms for the capacity fading of lithium-ion batteries (LIBs). Although significant efforts have been devoted to elucidating the origins of TM dissolution, its crosstalk effect on the anode interface is unclear, especially for its specific chemical state and electrochemical behavior. Herein, the interplay between the dissolved Mn²⁺ and the solid electrolyte interphases (SEI) on graphite anode is revealed by different characterization techniques, such as Raman spectroscopy, cryogenic transmission electron microscopy, electron energy loss spectroscopy, and time-of-flight secondary ion mass spectrometry. The results demonstrate that Mn2+ is inclined to coordinate with ethylene carbonate (EC), which is easily decomposed and generates organic-Mn²⁺ species and gaseous byproducts. These gases disrupt the SEI structure, facilitate electrolyte infiltration, and induce continuous growth of the SEI layer. This study deepens the understanding of TM crosstalk on SEI properties and LIB performance, offering potential strategies for enhancing battery durability and performance.

1. Introduction

Lithium transition metal oxide (LTMO) cathodes are widely employed in lithium-ion batteries (LIBs) for electronic devices and electric vehicles due to their high energy density, excellent rate performance, and low cost.^[1-4] However, transition metal (TM) crosstalk, especially Mn²⁺, significantly reduces battery performance and lifespan.^[5-10] Although it has been pointed out that the crosstalk of Mn²⁺ has the potential to destroy and reconstruct the solid electrolyte interphase (SEI) layer, leading to SEI

accumulation and capacity fading, the underlying mechanism is still controversial, especially for the specific chemical state of Mn (2+ or 0) in the SEI layer (Table S1, Supporting Information).[11–20]

Given the higher standard redox potential of Mn²⁺/Mn⁰ (1.87 V vs Li⁺/Li) compared to lithiated graphite (Gr,<0.2 V vs Li⁺/Li), Mn²⁺ is believed to be reduced to metallic Mn (Mn⁰) and deposited on the anode surface, which accelerates the electrolyte decomposition and Li+ consumption by enhancing the electronic conductivity of the SEI layer.[11,13,14] Delacourt et al., proposed that Mn²⁺ from the electrolyte is first reduced to Mn⁰ and subsequently oxidized through reactions with solvents during cycling.[13] This redox cycling will form cracks and porosity within the SEI layer, impairing passivation and promoting electrolyte decomposition and SEI growth.

Alternatively, other studies suggested that Mn⁰ deposits on the Gr interface act as catalytic centers that decompose lithium alkyl carbonates into Li₂CO₃ and other inorganic compounds. This catalytic process generates cracks and pores, leading to localized SEI growth at Mn⁰ deposition sites.^[12,15] Another perspective proposed that Mn²⁺ deposited in the SEI through ion-exchange reactions occupies Li⁺ positions and forms Mn(OCOR)₂, MnF₂, and MnCO₃, which blocks Li⁺ transport pathways, increasing interfacial resistance and causing capacity fade.^[16,18] Recent studies demonstrated that the solvation structure of Mn²⁺ with

C. Zhong, S. Niu, L. Wang, Y. Li, C. Zhan
State Key Laboratory of Advanced Metallurgy
University of Science and Technology Beijing
Beijing 100083, China
E-mail: liyejing@ustb.edu.cn; zhanchun@ustb.edu.cn
C. Zhong, S. Niu, L. Wang, Y. Li, C. Zhan
Department of Energy Storage Science and Engineering
School of Metallurgical and Ecological Engineering
University of Science and Technology Beijing
Beijing 100083, China

The ORCID identification number(s) for the author(s) of this article can be found under https://doi.org/10.1002/aenm.202503489

DOI: 10.1002/aenm.202503489

C. Zhong, Y. Li, S. Weng, J. Zhu, Z. Wang, H. Li, X. Wang Beijing National Laboratory for Condensed Matter Physics Institute of Physics Chinese Academy of Sciences Beijing 100190, China E-mail: wxf@iphy.ac.cn J. Zhu, Z. Wang, X. Wang

College of Materials Science and Opto-Electronic Technology University of Chinese Academy of Sciences Beijing 100049, China

T. Feng, X. Han, S. Wang Contemporary Amperex Technology Co. Ltd Ningde 352100, China

E-mail: WangSF01@catl-21c.com

ADVANCED ENERGY MATERIALS 16146840, 0. Downloaded from https://advanced.onlinelibrary.wiley.com/doi/10.1002/mem.202503489 by Institute Of Physics Chinese Academy Of Sciences, Wiley Online Library on [01/10/2025]. See the Terms and Conditions (https://onlinelibrary.wiley.com/emin/abunded from https://advanced.onlinelibrary.wiley.com/emin/abunded from https://a

solvent molecules (e.g., ethylene carbonate, EC) plays a critical role in determining battery performance than the traditionally-emphasized SEI effects. [20–22] Computational results indicate that Mn²⁺ solvation reduces the stability of the electrolyte, catalyzing its reduction and deposition on the SEI layer as MnCO₃. [20] The debating results on the correlation between the Mn²⁺ deposit and the performance degradation raise two critical questions: 1) How is Mn²⁺ deposited on the Gr anode, and what is the SEI layer's composition and morphology formed in the Mn²⁺ containing electrolytes? 2) How does the dissolved Mn²⁺ drive SEI layer growth?

Herein, the interplay between the dissolved Mn²⁺ and SEI layer of the Gr anode was explored by using practical LiFePO₄||Gr (LFP||Gr) pouch cells with the addition of 2500 ppm Mn²⁺ on purpose. The evolution of the Gr SEI layer was characterized by various techniques, including X-ray photoelectron spectroscopy (XPS), cryogenic transmission electron microscopy (Cryo-TEM), electron energy loss spectroscopy (EELS), and timeof-flight secondary ion mass spectrometry (ToF-SIMS). Additionally, the solvation behavior of Mn2+ in the electrolyte and its decomposition pathways were elucidated using Raman spectroscopy and differential electrochemical mass spectrometry (DEMS). Our results reveal that the participation of Mn²⁺ in the solvation structure significantly alters the electrochemical behavior of the electrolyte and the stability of the SEI layer. Specifically, Mn²⁺ competes with Li⁺ for coordination with solvent molecules (e.g., EC), forming EC-Mn²⁺ solvation complexes with lower reduction stability compared to EC-Li+ complexes. This instability promotes the generation of organic-Mn²⁺ species and gaseous byproducts (e.g., CO₂, C₂H₄, CO). The formation of gases further destabilizes the SEI layer, facilitating continuous electrolyte infiltration and decomposition during cycling, ultimately leading to SEI growth (≈49 nm after 1000 cycles compared to 20 nm for the base electrolyte). These Mn²⁺-induced processes contribute to increased gas evolution, SEI growth, and ultimately, capacity fading in lithiumion batteries. This study provides critical insights into the role of Mn²⁺ dissolution in battery degradation, proposing potential strategies to mitigate such effects via electrolyte engineering or SEI stabilization, thereby enhancing battery performance and longevity.

2. Results and Discussion

2.1. Electrochemical Performance with Mn2+ Additive

LFP was used as the cathode material due to its exceptional cycling stability, negligible degradation, and minimal transition metal dissolution, ensuring that the observed degradation in the electrochemical performance could be primarily associated with the Gr anode. To simulate and magnify the electrochemical behavior of Mn²⁺ dissolution, Mn²⁺ (derived from Mn(TFSI)₂) was added to the base electrolyte (1 mol L⁻¹ LiPF₆ in EC/dimethyl carbonate (DMC) (3:7 ww) + 2 wt.% vinylene carbonate (VC)). The presence of TFSI⁻ in the electrolyte was proved to have a negligible effect on the electrochemical performance of the LFP||Gr batteries (Figure S1a, Supporting Information). LFP||Gr pouch cells were assembled using both the base electrolyte (referred to as "base") and the Mn²⁺-containing

electrolyte (referred to as "concentration Mn", e.g., "2500 ppm Mn"). Since higher Mn²⁺ content leads to faster capacity degradation (Figure S1b, Supporting Information), 2500 ppm Mn²⁺ is selected for further study to exacerbate the effect of Mn²⁺ on the Gr anode, which is consistent with the Mn content detected on the anode of the LiMn₂O₄||Gr (LMO||Gr) pouch cell (Figure S2 and Table S2, Supporting Information). Figure 1a shows that the battery capacities gradually increase, reflecting the dynamic activation process. After 20 cycles, the capacities are stabilized, and the coulombic efficiency consistently approaches 99.8% (Figure S3a, Supporting Information). Notably, after 1000 cycles, the batteries utilizing the base electrolyte and the 2500 ppm Mn electrolyte display capacity retention of 91.22% and 84.35% at 0.33C (Figure 1a), respectively. The first charging curve of the cell with the 2500 ppm Mn shows a plateau at 1.2 V (Figure 1b), suggesting a potential reduction of Mn2+ on Gr and resulting in a lower initial CE of 87.07% (compared to 91.42% for the base electrolyte). Furthermore, the continuous capacity decay (Figure \$3b,c, Supporting Information) of the cell with the 2500 ppm Mn highlights the persistent detrimental effect of Mn²⁺ on the cycling stability.

The EIS was conducted in a three-electrode cell to differentiate the resistance contribution from the cathode and the anode. The EIS spectrum can be divided into three distinct regions (Figure 1c): the diffusion impedance of Li⁺ through the SEI layer in the high-frequency region (1 kHz < f < 10 kHz), the charge-transfer impedance in the mid-frequency region (1 Hz < f < 1 kHz), and the Warburg diffusion impedance in the low-frequency region (f < 1 Hz)^[25] As illustrated in Figure 1c and Figure S4 (Supporting Information), the Gr anode cycled in the 2500 ppm Mn electrolyte (referred to as "2500 ppm Mn Gr") exhibits significantly higher SEI resistance compared to the Gr anode cycled in the base electrolyte (referred to as "base Gr"). Specifically, the SEI resistance in the 2500 ppm Mn Gr increases markedly from 0.0151 Ω after 50 cycles to 0.0166Ω after 150 cycles, indicating continuous SEI growth or the formation of high-resistance components. In contrast, the SEI resistance in the base Gr shows only a slight increase from 0.0127 to 0.0131 Ω over the same cycling period (Figure 1d; Table S3, Supporting Information). Furthermore, the cathode resistance remains nearly unchanged throughout cycling (Figure S4b,e, Supporting Information), confirming that the capacity fading of the pouch cell is primarily attributed to anode degradation rather than cathode-related is-

2.2. SEI Chemistry

The chemical compositions of the SEI layers at different cycles on Gr electrodes were detected by XPS. The intensity of C–O (286.4 eV) in the SEI layer of 2500 ppm Mn Gr is significantly higher than that in the base Gr (Figure 2a,b), indicating that more solvent molecules are reduced to form organics in the 2500 ppm Mn electrolyte. Furthermore, after 100 cycles, the C–O amount on the 2500 ppm Mn Gr significantly increases from 21% (formation) to 37%, whereas it only rises from 23% to 28% for the SEI layer on the base Gr (Figure 2e). Similarly,

16 146840, 0, Downloaded from https://advanced.co.inlinelibrary.wiley.com/doi/10.1002/zemm.0202503489 by Institute Of Physics Chinese Academy Of Sciences, Wiley Online Library on [01/10/2025]. See the Terms and Conditions (https://onlinelibrary.wiley.com/en/inline

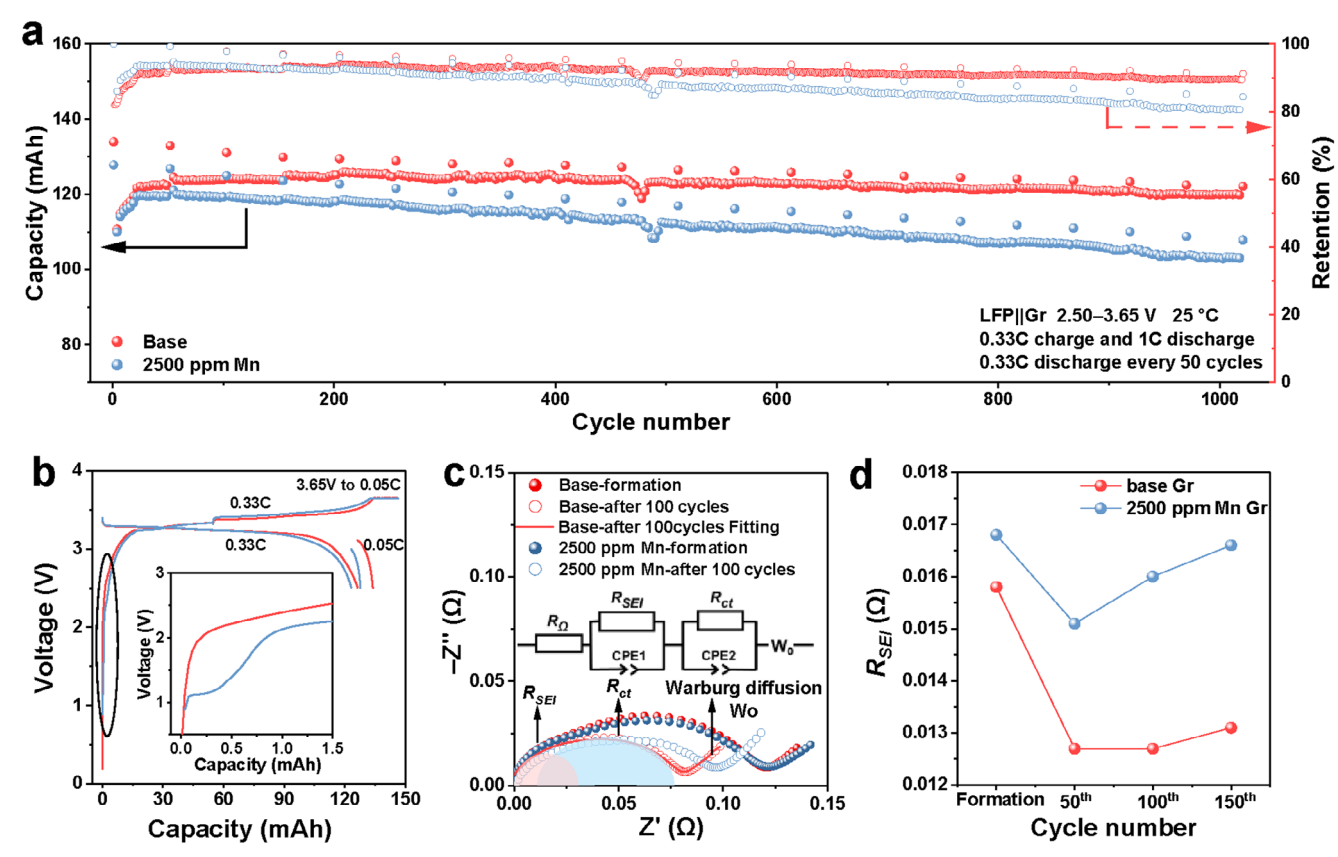


Figure 1. a) Cycling performance and capacity retention of the LFP||Gr pouch cells with base electrolyte and 2500 ppm Mn electrolyte. The filled circles represent the capacity, and the hollow circles represent the capacity retention of LFP||Gr pouch cells. b) The first charge—discharge curves of the LFP||Gr pouch batteries with the base electrolyte and 2500 ppm Mn electrolyte. The inset shows a voltage profile of the initial stage of battery charging taken from the black ellipse. c) EIS spectra of Gr||Li with base electrolyte and 2500 ppm Mn electrolyte from the three-electrode pouch cells. The inset shows the resistance assignment and the equivalent circuit model for fitting. d) The fitting results of R_{SFI} in Gr||Li based on Table S3 (Supporting Information).

after 100 cycles, the LiF amount on the 2500 ppm Mn Gr significantly increases from 14% (formation) to 40% (Figure 2c,d), compared to a modest increase from 18% to 21% for the SEI layer on the base Gr (Figure 2f). These results indicate that the SEI layer formed in 2500 ppm Mn electrolyte is less effective in passivating the Gr surface, thereby failing to suppress continuous electrolyte decomposition during cycling. These findings collectively demonstrate that Mn²⁺ promotes additional parasitic reduction reactions of the electrolyte on the Gr surface. Furthermore, the Mn 2p XPS spectrum (Figure \$5, Supporting Information) confirms the presence of Mn²⁺ on the 2500 ppm Mn Gr with Mn 2p_{3/2} binding energy at 641.4 eV, and multiplet splitting of 11.8 eV (Figure S5, Supporting Information), which is close to that of MnO.[26] The existence of the satellite feature indicates that Mn exists in the +2 oxidation state within the SEI layer.

2.3. SEI Nanostructure

The nanostructure and compositional distribution of the SEI layers are shown in **Figure 3** and Figures S6–S14 (Supporting Information) (enlarged images in Figure 3). In the 2500 ppm Mn Gr, the SEI layers exhibit a mosaic-like structure, charac-

terized by crystalline inorganic nanograins embedded within an amorphous matrix, and an increased thickness of ≈12 nm after the initial formation process (Figure 3e; Figure S10, Supporting Information). In contrast, the SEI layer on the base Gr displays a predominantly amorphous structure with a thickness of ≈8 nm (Figure 3a; Figure S6, Supporting Information). This distinct structural difference indicates that the presence of Mn²⁺ alters the decomposition pathways of the electrolyte, leading to the formation of a more complex SEI layer. In the 2500 ppm Mn Gr, the SEI layers maintain a mosaiclike structure, and the thickness increases to ≈17 nm after 50 cycles (Figure 3f; Figure S11, Supporting Information). This contrasts with the SEI layers on the base Gr, which remain predominantly amorphous. Notably, its thickness exhibits a gradual increase: from 8 nm at the 50th cycle to 14 nm at the 100th cycle, and further to 20 nm at the 1000th cycle. (Figure 3b-d). The mosaic-like structure on the 2500 ppm Mn Gr is attributed to the complete decomposition of organic components in the electrolyte, accompanied by gas release (e.g., CO2, CO, and C2H4), which generates inorganic phases in the porous SEI layer and thus facilitates continuous electrolyte penetration and decomposition at the Gr surface. As a result, the SEI layer thickness in the 2500 ppm Mn Gr further increases to 50 nm after 1000 cycles (Figure 3h).

16146840, 0, Downloaded from https://advanced.onlinelibrary.wiley.com/doi/10.1002/ænm.202503489 by Institute Of Physics Chinese Academy Of Sciences, Wiley Online Library on [01/10/2025]. See the Terms and Conditions (https://onlinelibrary.wiley

.com/terms-and-conditions) on Wiley Online Library for rules of use; OA articles are governed by the applicable Creative Commons License

www.advenergymat.de

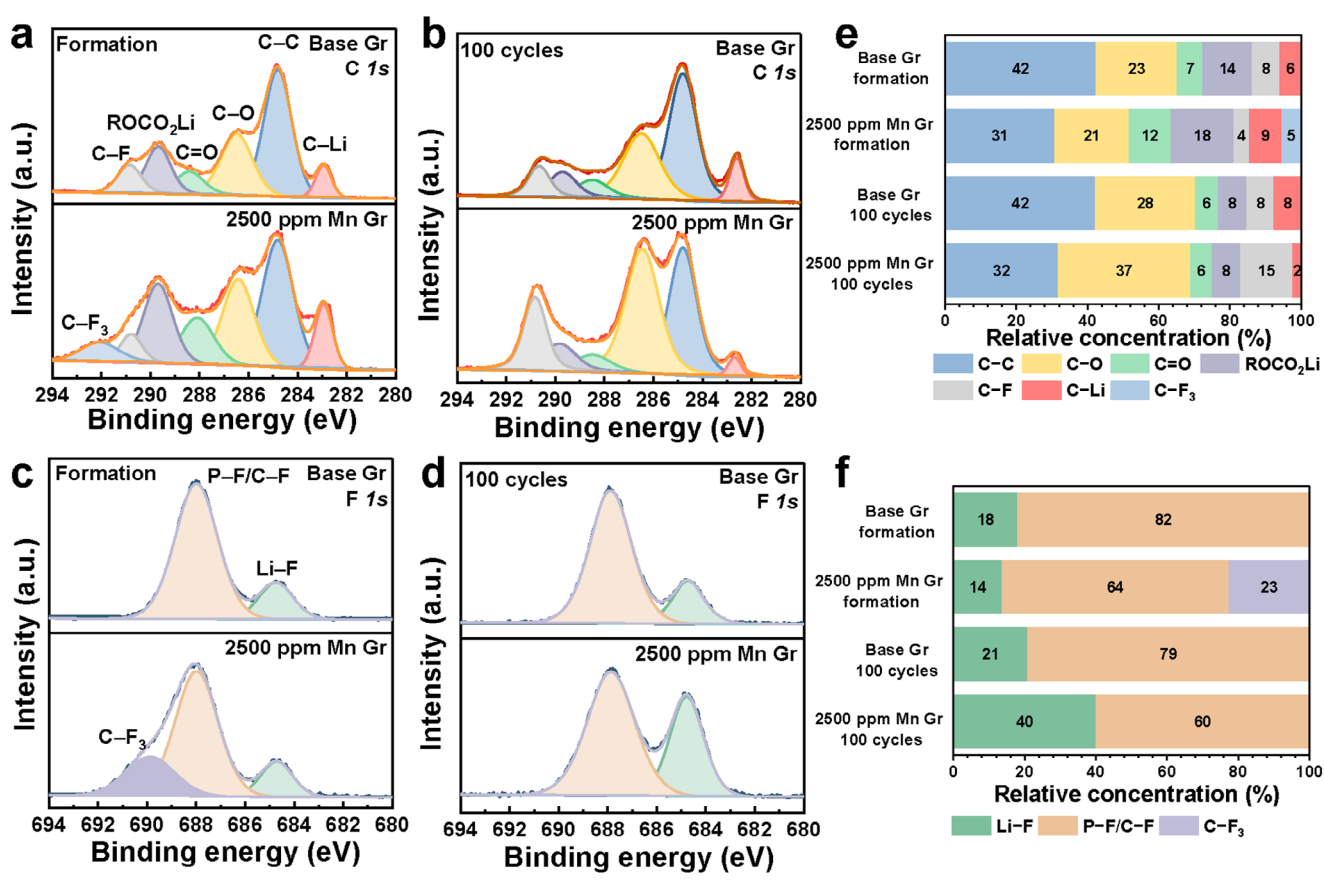


Figure 2. a,b) C 1s XPS spectra for 2500 ppm Mn Gr and base Gr after formation (a) and 100 cycles (b). c,d) F 1s XPS spectra for 2500 ppm Mn Gr and base Gr after formation (c) and 100 cycles (d). e,f) The relative concentration ratio of different components based on C 1s spectra (e) and F 1s spectra (f).

Although XPS analysis confirms the presence of Mn^{2+} within the SEI layer, no lattice fringes assignable to crystalline Mn^{2+} containing compounds (e.g., MnO, MnCO₃, or MnF₂) were observed in TEM images (Figure 3). Additionally, despite the theoretical expectation of metallic Mn° formation within the SEI layer, the crystalline domains of Mn^{0} were undetected, even in the lithiated Gr (Figure 3i; Figure S14, Supporting Information).

To further investigate the chemical state and spatial distribution of Mn within the SEI layer, EELS analysis was conducted (Figure 3j; Figure S15, Supporting Information). The oxidation state of Mn was determined by calculating the intensity ratio between the L_3 (644.5 eV) and L_2 (656.2 eV) peaks in the Mn L-edge EELS spectra.^[27] The results confirm that Mn exists predominantly in the +2 oxidation state in both lithiated and delithiated Gr (Figures \$15 and \$16, Supporting Information). EELS mapping further reveals that the Mn²⁺ distribution within the SEI layer is independent of cycling. Specifically, Mn is primarily localized in the outer layer of the SEI, accompanied by carbon (C) elements, while its presence in the inner layer is significantly reduced (Figure 3k,l). This spatial distribution pattern remains consistent even as the cycle number increases.

2.4. Specific Mn²⁺ Compounds in the SEI Layer

The ToF-SIMS was employed to further investigate the composition and distribution of Mn²⁺ within the SEI layer by analyzing characteristic functional group fragments (Figure 4; Figure \$17, Supporting Information). Figure 4a,b presents the normalized depth profiles of characteristic ionic fragments of inorganic (e.g., LiF₂-), organic (e.g., CH₃O-) components, and bulk Gr (C⁻).[28] The SEI layer on the 2500 ppm Mn Gr exhibits a larger thickness compared to the base Gr (99 vs 76 s sputtering time), which aligns with the cryo-TEM results. This further supports the conclusion that the presence of Mn²⁺ in the electrolyte accelerates SEI growth during cycling. Notably, the depth profiles reveal a strong overlap between the distributions of CH₃O⁻ fragments and Mn⁻ fragments, indicating the formation of organic-Mn²⁺ species within the SEI layer. This observation is consistent with the co-localization of Mn and C signals observed in the EELS mapping, suggesting that Mn²⁺ combines with organic components to form stable compounds. The reconstruction images in Figure 4d further demonstrate a strong spatial correlation between Mn⁻ and CH₃O⁻ fragments. This resolves the discrepancy between the Mn²⁺ observed via XPS and the absence of crystalline Mn²⁺-containing compounds in TEM, indicating that Mn within the SEI layer primarily exists in amorphous form, likely as

Academy Of Sciences, Wiley Online Library on [01/10/2025]. See the Terms

on Wiley Online Library for rules of use; OA articles are governed by the applicable Creative Commons

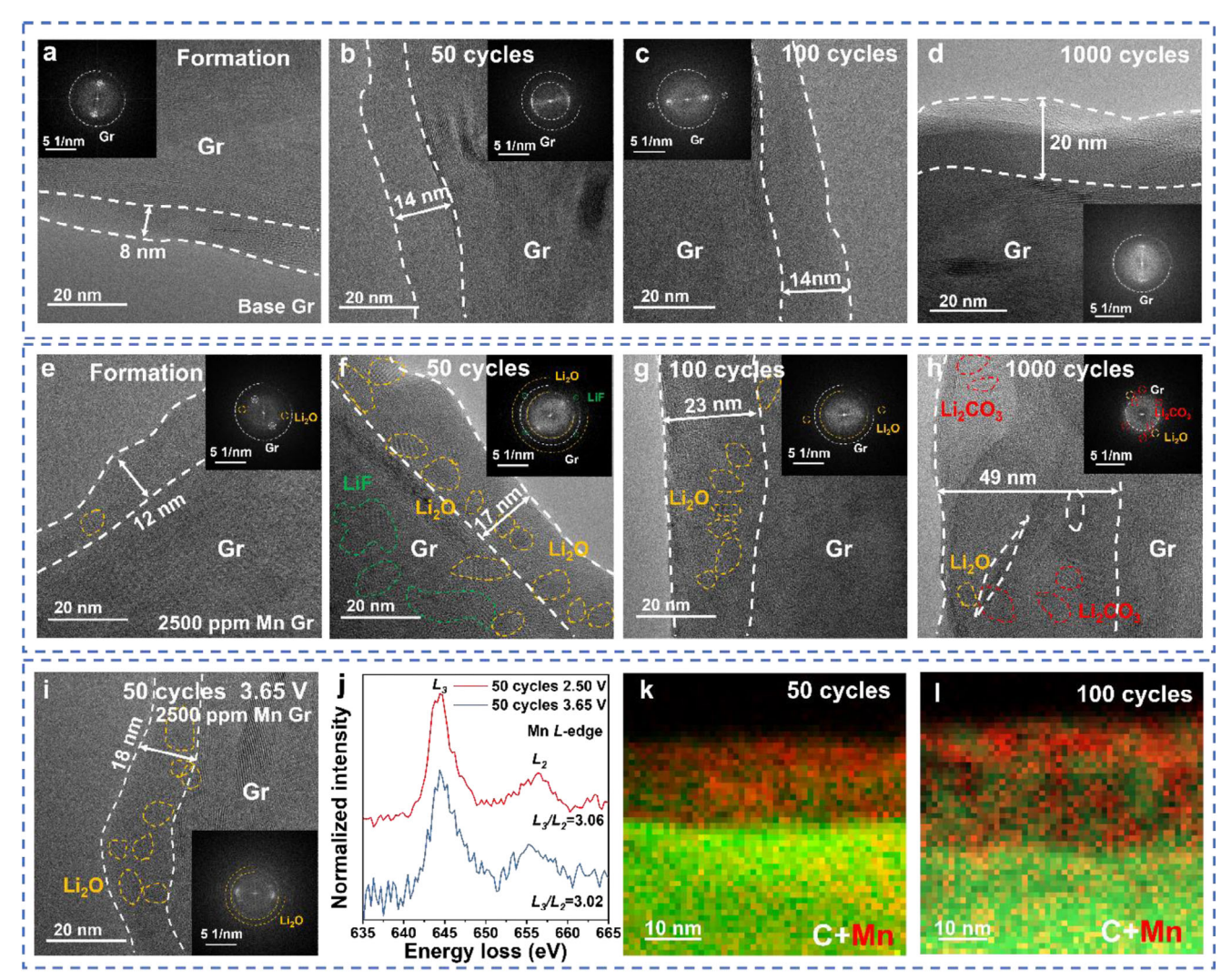


Figure 3. a–d) Cryo-TEM images and (inset) their fast-Fourier transform (FFT) patterns of SEI layers on base Gr after formation, 50 cycles, 100 cycles, and 1000 cycles. e–h) Cryo-TEM images of SEI layers on 2500 ppm Mn Gr after formation, 50 cycles, 100 cycles, and 1000 cycles. i) Cryo-TEM image of SEI layer on the lithiated 2500 ppm Mn Gr (the pouch cell was charged to 3.65 V). j) The EELS of Mn *L*-edge on the lithiated Gr and delithiated (the pouch cell was discharged to 2.50 V) 2500 ppm Mn Gr. k,l) EELS mappings showing the distribution of carbon (C) and Mn on the delithiated 2500 ppm Mn Gr after 50 and 100 cycles. Color code: C, green; Mn, red.

organic-Mn²⁺ complexes. Moreover, the SEI layer formed in the 2500 ppm Mn²⁺ electrolyte exhibits a non-uniform distribution of organic and inorganic components, suggesting that Mn²⁺ promotes heterogeneous electrolyte decomposition on the Gr surface during cycling. In contrast, the SEI layer formed in the base electrolyte displays a homogeneous outer layer, with a more uniform distribution of organic and inorganic phases (Figure 4c).

2.5. Solvation Structure and Decomposition Pathways of Electrolytes

The above varied SEI layer composition and structure with/without Mn^{2+} is closely tied to the solvation structure of the electrolyte. Therefore, elucidating the solvation behavior of Mn^{2+} in the electrolyte is essential. Due to the low Mn^{2+}

concentration in a 2500 ppm Mn electrolyte, direct observation of the coordination interactions between Mn2+ and solvent molecules was not feasible by Raman spectroscopy (Figure S18, Supporting Information). Therefore, a higher Mn²⁺ concentration of 0.3 mol L⁻¹ (referred to as "0.3 M Mn"; Figure 5a) was prepared and tested. The addition of Mn²⁺ causes a shift in the ethylene carbonate solvation (EC-Li+/Mn2+) peak to a higher wavenumber (from 727 cm⁻¹ in the base electrolyte to 729 cm⁻¹ in the 0.3 M Mn electrolyte), while other peaks remained unchanged (Figure S19, Supporting Information). This shift suggests that Mn²⁺ enters or replaces the EC-Li⁺ solvation shell (Figure 5b), forming an EC-Mn²⁺ solvation structure (Figure 5c).^[20] Calculation results show that the binding energy (B.E.) of Mn^{2+} with EC (-14.713 eV) is more negative than that of Li⁺ with EC (-5.594 eV), indicating a stronger interaction between EC and Mn²⁺. Furthermore, the EC-Mn²⁺ possesses

16146840, 0. Downloaded from https://advanced.onlinelibrary.wiley.com/doi/10.1002/mem.202503489 by Institute Of Physics Chinese Academy Of Sciences, Wiley Online Library on [01/10/2025]. See the Terms and Conditions (https://onlinelibrary.wiley.com/emin/abunded from https://advanced.onlinelibrary.wiley.com/emin/abunded from https://a

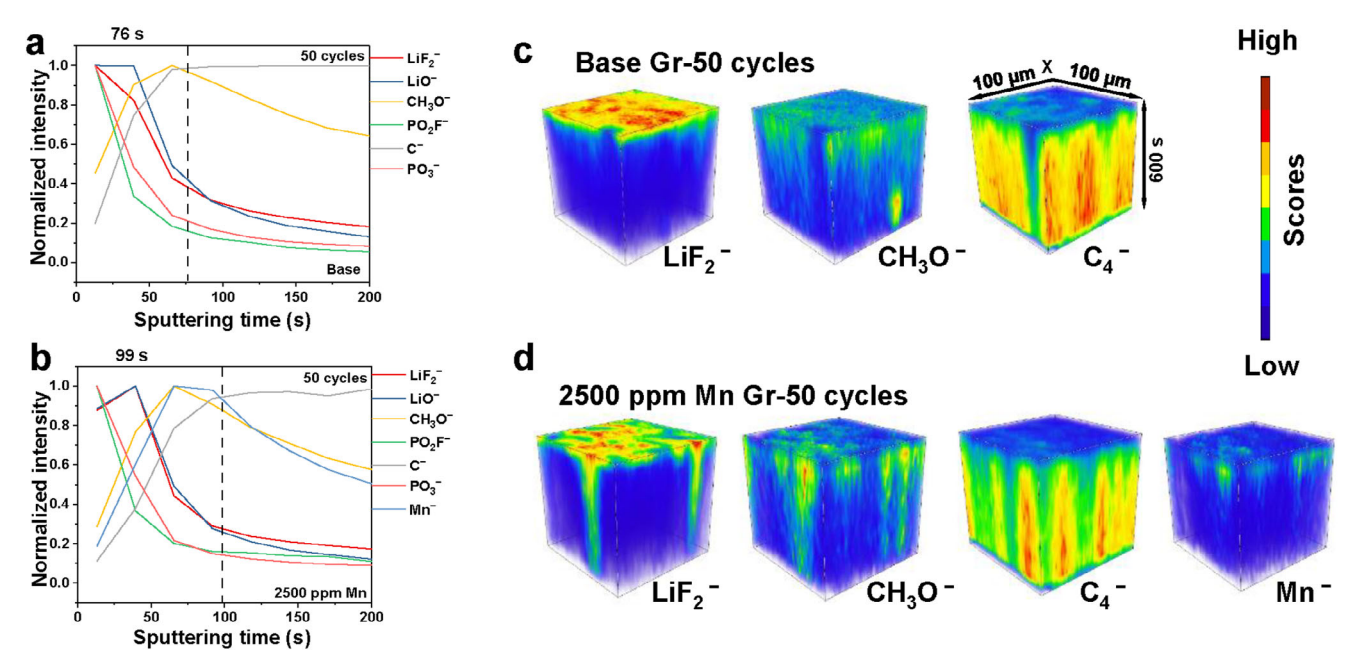


Figure 4. a,b) Normalized ToF-SIMS depth profiles of some selected fragments sputtered from the base Gr (a) and 2500 ppm Mn Gr (b) after 50 cycles. c,d) 3D structure of some selected fragments sputtered from the base Gr (c) and 2500 ppm Mn Gr (d) after 50 cycles.

a lower Lowest Unoccupied Molecular Orbital (LUMO) energy than EC-Li⁺ (Figure 5b,c), which renders them more susceptible to decomposing.^[22] This finding aligns with the presence of Mn²⁺ with organic components in the SEI layer. Linear sweep voltammetry (LSV) was employed to evaluate the electrochemical stability of electrolytes (Figure 5d). In the base electrolyte, a reduction peak is observable ≈0.7 V (vs Li⁺/Li), which corresponds to the formation of the SEI layer due to the reduction of the EC-Li⁺.^[29] In contrast, the 2500 ppm Mn electrolyte exhibits an additional reduction peak at ≈ 1.2 V, attributed to the reduction of EC-Mn²⁺ complexes. Furthermore, the LSV curves show an increased current response at the electrolyte reduction potential, indicating that the introduction of Mn2+ lowers the electrochemical stability of the electrolyte and accelerates reduction reactions. This behavior explains the distinct SEI layer properties observed in the presence of Mn^{2+} .

Additionally, the LFP||Gr pouch cell cycled in the 2500 ppm Mn electrolyte demonstrates significant volume expansion after cycling (Figure S20, Supporting Information), which is linked to the gas generation caused by Mn²⁺-induced electrolyte decomposition. In situ DEMS was carried out to directly monitor the gaseous byproducts generated during electrolyte reduction in operating batteries. The released gases were detected as H2, CO2, C_2H_4/CO , and CH_4 in the early stage of charging (Figure 5e,f), which are related to electrolyte decomposition to form the SEI layer at the anode side. The CH₄ is mainly derived from linear carbonates containing methyl groups (Reaction (1)), such as DMC.[30,31] Given the small amount of H₂O in the electrolyte, H₂ is mainly from the decomposition of the protonated solvent (Reaction (2)).[32] Although it cannot separate the gases from the C₂H₄ or CO, it can attribute them to the products of solvent decomposition (Reaction (3) and (4)), such as EC.[30,31,33] In the 2500 ppm Mn electrolyte, the intensity of all gases, particularly

CO₂ and C₂H₄/CO, increases almost instantaneously during the initial charging stage. This behavior contrasts sharply with that observed in the base electrolyte, where CO2 and H2 concentrations rise rapidly at the beginning of charging, while C2H4/CO and CH₄ show only a slight increase. In the base electrolyte, CO₂ and H₂ are the dominant gaseous products. The distinct gas evolution in the 2500 ppm Mn electrolyte suggests that the addition of Mn²⁺ modifies the reduction pathways of the electrolyte (Reactions (5) and (6)). Based on the timing of its formation, potential electrolyte reduction pathways are proposed, as illustrated in Figure 5g and Figure S21 (Supporting Information). With the involvement of Mn²⁺, solvent molecules likely undergo Reactions (5) and (6), generating CO and CO2 gases along with organic compounds containing C-O bonds. These findings are consistent with the XPS results shown in Figure 2b, which indicate the presence of organic species with C-O bonds in the SEI layer. Additionally, other EC molecules in the solvent shell (Figure 5c) participate in Mn²⁺-mediated reduction processes, forming Li₂O and releasing gaseous byproducts such as CO2 and C2H4 (Figure **S21**, Supporting Information).

2.6. Interplay Between the Mn^{2+} and $Gr\ SEI\ Layer$

Previous work suggested that Mn²⁺ in the electrolyte would be reduced to Mn⁰ through (electro)chemical reactions and deposited on the anode surface, which exhibits catalytic activity and catalyzes electrolyte decomposition.^[13,15,34,35] According to this mechanism, the SEI layer would continuously grow outward from Mn²⁺-containing active sites, which is different from the bottom-up growth mode observed in this work. Based on DFT calculation, Xing et al.,^[20] suggested that Mn²⁺ in the electrolyte can catalyze the decomposition of PF₆⁻ anions into

6146840, 0, Downloaded from https://advanced.onlinelibrary.wiley.com/doi/10.1002/ænm.202503489 by Institute Of Physics Chinese Academy Of Sciences, Wiley Online Library on [01/10/2025]. See the Terms and Condit

and-conditions) on Wiley Online Library for rules of use; OA articles are governed by the applicable Creative Commons License

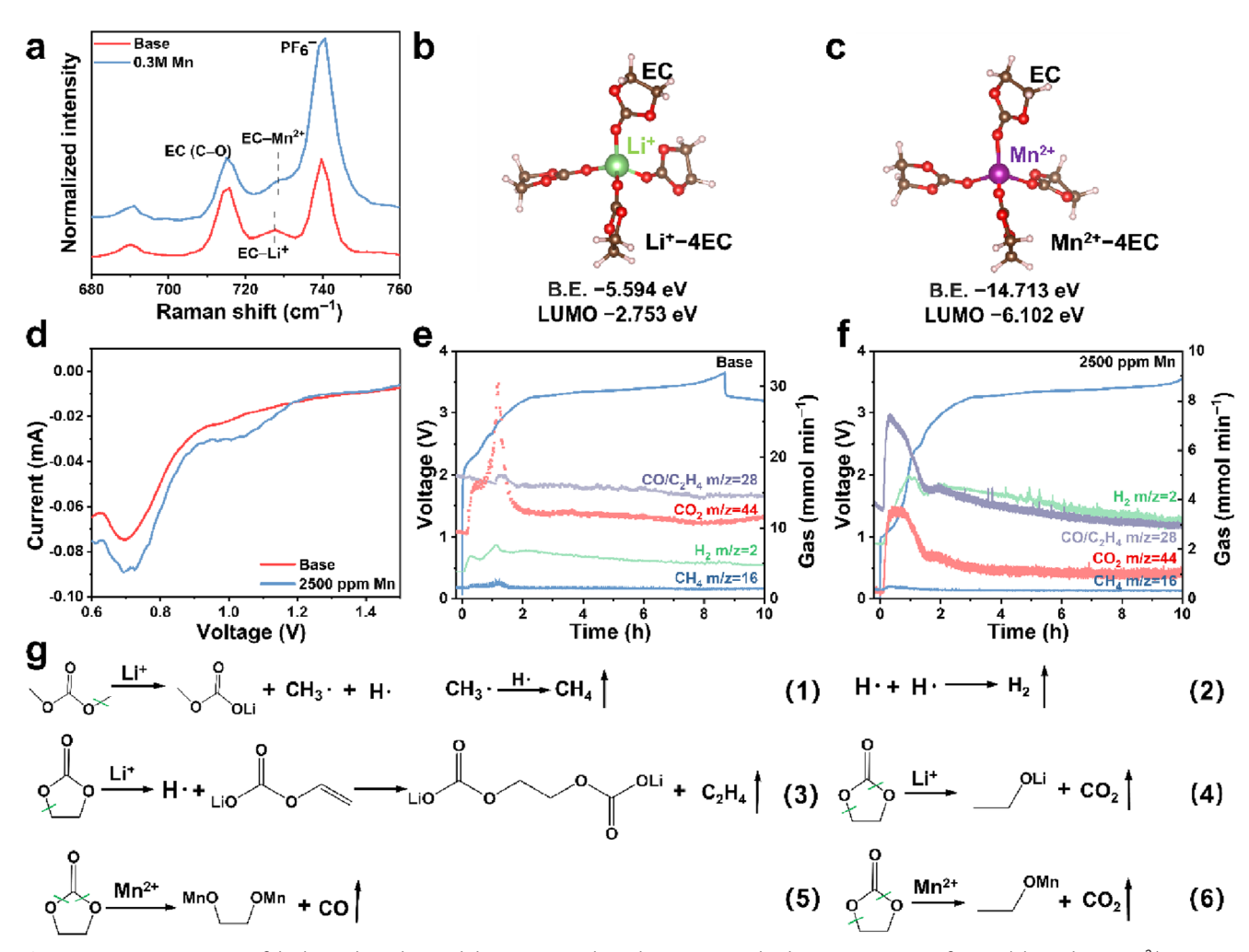


Figure 5. a) Raman spectra of the base electrolyte and the 0.3 м Mn electrolyte. Optimized solvation structures of EC–Li⁺ b) and EC–Mn²⁺ c). Atom color code: C, brown; H, white; O, red; Li, green; and Mn, purple. d) The LSV curves of Li||Gr half-cell with base electrolyte and 2500 ppm Mn electrolyte. e,f) Voltage curves of LFP||Gr cell and the corresponding gas evolution during the first cycle with base electrolyte and 2500 ppm Mn electrolyte through in situ DEMS. g) The potential pathways for the decomposition of DMC and EC in base electrolyte and 2500 ppm Mn electrolyte.

phosphorus pentafluoride (PF₅) with high catalytic activity, which further catalyzes the decomposition of carbonate solvent molecules to form MnCO₃. However, MnCO₃ was not detected in our experiments.

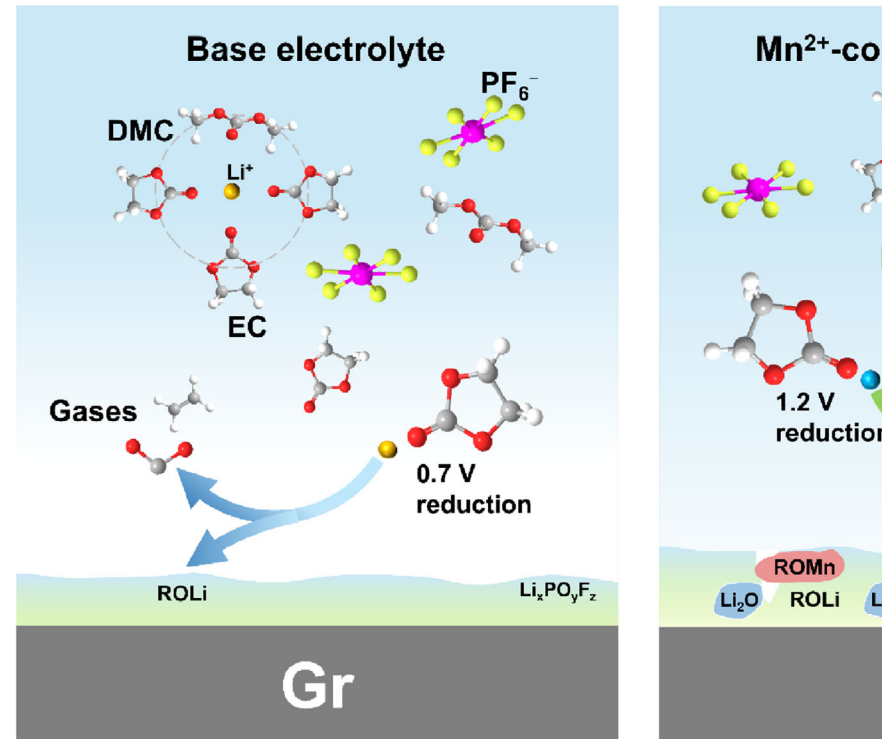
Based on the above XPS, cryo-TEM, ToF-SIMS, and Raman results, a proposed mechanism for the interplay between Mn²⁺ and Gr SEI layer is shown in **Figure 6**. Dissolved Mn²⁺ alters the chemical environment of the electrolyte through preferential coordination with solvents, such as EC-Mn²⁺, as probed by Raman spectroscopy (Figure 5a). Such solvation structure change elevates the reduction potential of the electrolyte and alters its reaction pathway (Figure 5d). More organics (e.g., C-O species) were detected by XPS as well as the signals from Mn²⁺ (Figure 2a; Figure S4, Supporting Information). Since cryo-TEM didn't find any lattice fringes attributable to crystalline Mn²⁺ containing compounds (Figure 3e-h), the Mn²⁺ deposit is predominantly incorporated in amorphous SEI components, to be specific, organic-Mn²⁺ complexes, as confirmed by ToF-SIMS.

In situ DEMS demonstrates substantial gas evolution (e.g., CO_2 , CO, and C_2H_4) during the reduction of Mn^{2+} -containing electrolyte. These gases disrupt the integrity of the SEI layer, creating pathways for continuous electrolyte infiltration and further reactions at the Gr/SEI interface, consistent with EELS-mapping and ToF-SIMS observations of Mn enrichment at the SEI outermost layer (Figures 31 and 4d). As a result, the SEI layer grows predominantly from the bottom up, leading to progressive thickening over cycling. This accumulation of SEI hinders interfacial Li+ transport, leading to increased resistance and reduced capacity as active Li⁺ is consumed. In contrast, the decomposition of the base electrolyte forms organic-Li species (e.g., ROLi) accompanied by a small amount of gas (e.g., CO₂ and C₂H₄), underscoring the distinct and detrimental role of Mn²⁺ in regulating the SEI layer formation and battery performance. Thus, future work should focus on two points to reduce the harmful influence induced by Mn²⁺: i) adopting the electrolyte with a lower binding energy between Mn²⁺ and the solvents, ii) forming a dense SEI

46840, 0, Downloaded from https://advanced.onlinelibrary.wiley.com/doi/10.1002/aenm.202503489 by Institute Of Physics Chinese

Academy Of Sciences, Wiley Online Library on [01/10/2025]. See the Terms

on Wiley Online Library for rules of use; OA articles are governed by the applicable Creative Commons License



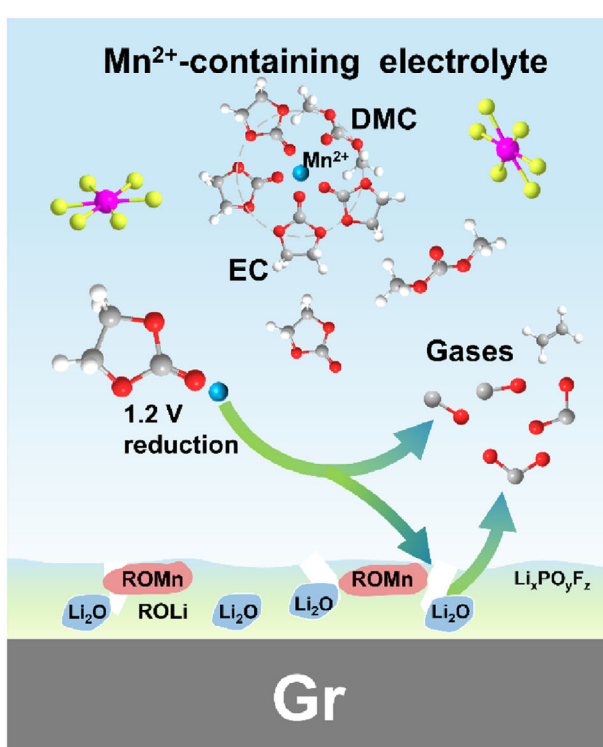


Figure 6. Schematic illustration comparing the electrolyte reduction mechanisms and SEI structures in the base electrolyte and Mn^{2+} -containing electrolyte.

layer with better electronic insulation to inhibit further electrolyte reduction following Mn^{2+} dissolution.

3. Conclusion

In this study, a suite of advanced characterization techniques, including XPS, ToF-SIMS, and Cryo-TEM, was employed to comprehensively analyze the evolution of interfacial properties across various cycles and to probe the impact of transition metal Mn²⁺ on the SEI layer. The presence of Mn²⁺ in the electrolyte significantly alters the solvation structure and reduction pathways, leading to distinct SEI properties and accelerated electrolyte decomposition. Mn²⁺ competes with Li⁺ for coordination with solvent molecules (e.g., EC), forming EC-Mn²⁺ solvation complexes that are more prone to reduction. This promotes the generation of organic-Mn²⁺ species and gaseous byproducts (e.g., CO₂, C₂H₄/CO), facilitating continuous electrolyte infiltration and decomposition, resulting in a thicker, mosaic-like SEI layer. These Mn²⁺-induced processes contribute to increased gas evolution, SEI growth, and ultimately, capacity fading in LIBs. This study provides critical insights into the role of transition metal dissolution in battery degradation and offers potential strategies for mitigating these effects through electrolyte engineering or SEI stabilization, and improving battery performance and longevity.

Supporting Information

Supporting Information is available from the Wiley Online Library or from the author.

Acknowledgements

This work was financially supported by the National Key R&D Program of China (Nos. 2022YFB2502200 and 2021YFC2900900), the National Natural Science Foundation of China (Nos. 52172257, and 52502211), the Natural Science Foundation of Beijing Municipality (Nos. 2254076 and L247018), the China Postdoctoral Science Foundation (No. 2023M743739), and the Postdoctoral Fellowship Program of CPSF (No. GZC20232939).

Conflict of Interest

The authors declare no competing financial interest.

Data Availability Statement

The data that support the findings of this study are available in the supplementary material of this article.

Keywords

lithium-ion battery, Mn²⁺ dissolution, solid electrolyte interface growth, solvation structure

Received: June 25, 2025 Revised: September 24, 2025 Published online:

[1] A. Manthiram, J. C. Knight, S. T. Myung, S. M. Oh, Y. K. Sun, Adv. Energy Mater. 2015, 6, 1501010.

/advanced.onlinelibrary.wiley.com/doi/10.1002/aenm.202503489 by Institute Of Physics Chinese

Academy Of Sciences, Wiley Online Library on [01/10/2025]. See the Terms

of use; OA articles are governed by the applicable Creative Commons License

www.advancedsciencenews.com www.advenergymat.de

- [2] M. M. Thackeray, K. Amine, Nat. Energy 2021, 6, 566.
- [3] Z. Cui, F. Zou, H. Celio, A. Manthiram, Adv. Funct. Mater. 2022, 32, 2203779.
- [4] W. Zeng, F. Xia, J. Wang, J. Yang, H. Peng, W. Shu, Q. Li, H. Wang, G. Wang, S. Mu, J. Wu, Nat. Commun. 2024, 15, 7371.
- [5] K. C. Harris, M. H. Tang, J. Chem. Phys. 2018, 122, 20632.
- [6] R. Jung, F. Linsenmann, R. Thomas, J. Wandt, S. Solchenbach, F. Maglia, C. Stinner, M. Tromp, H. A. Gasteiger, J. Electrochem. Soc. 2019, 166, A378.
- [7] Z. Zhang, S. Said, A. J. Lovett, R. Jervis, P. R. Shearing, D. J. L. Brett, T. S. Miller, ACS Nano 2024, 18, 9389.
- [8] X. Zhang, Z. Cui, A. Manthiram, Adv. Energy Mater. 2022, 12, 2103611.
- [9] Y. Song, L. Wang, L. Sheng, D. Ren, H. Liang, Y. Li, A. Wang, H. Zhang, H. Xu, X. He, *Energy Environ. Sci.* 2023, 16, 1943.
- [10] C. Zhan, T. Wu, J. Lu, K. Amine, Energy Environ. Sci. 2018, 11, 243.
- [11] S. Komaba, N. Kumagai, Y. Kataoka, Electrochim. Acta 2002, 47, 1229.
- [12] M. Ochida, Y. Domi, T. Doi, S. Tsubouchi, H. Nakagawa, T. Yamanaka, T. Abe, Z. Ogumi, J. Electrochem. Soc. 2012, 159, A961.
- [13] C. Delacourt, A. Kwong, X. Liu, R. Qiao, W. L. Yang, P. Lu, S. J. Harris, V. Srinivasan, J. Electrochem. Soc. 2013, 160, A1099.
- [14] S. R. Gowda, K. G. Gallagher, J. R. Croy, M. Bettge, M. M. Thackeray, M. Balasubramanian, Phys. Chem. Chem. Phys. 2014, 16, 6898.
- [15] T. Joshi, K. Eom, G. Yushin, T. F. Fuller, J. Electrochem. Soc. 2014, 161, A1915.
- [16] C. Zhan, J. Lu, A. Jeremy Kropf, T. Wu, A. N. Jansen, Y.-K. Sun, X. Qiu, K. Amine, Nat. Commun. 2013, 4, 2437.
- [17] X. Xiao, Z. Liu, L. Baggetto, G. M. Veith, K. L. More, R. R. Unocic, Phys. Chem. Chem. Phys. 2014, 16, 10398.
- [18] C. Zhan, X. Qiu, J. Lu, K. Amine, Adv. Mater. Interfaces 2016, 3, 1500856
- [19] H. Shin, J. Park, A. M. Sastry, W. Lu, J. Power Sources 2015, 284, 416.

- [20] C. Wang, L. Xing, J. Vatamanu, Z. Chen, G. Lan, W. Li, K. Xu, Nat. Commun. 2019, 10, 3423.
- [21] J. Zhang, W. Li, J. Wang, P. Wang, J. Sun, S. Wu, H. Dong, H. Ding, D. Zhao, S. Li, Electrochim. Acta 2022, 417, 140334.
- [22] X. Cui, J. Sun, D. Zhao, J. Zhang, J. Wang, H. Dong, P. Wang, J. Zhang, S. Wu, L. Song, N. Zhang, C. Li, S. Li, J. Energy Chem. 2023, 78, 381.
- [23] R. M. Torres, A. Manthiram, Small 2024, 20, 2309350.
- [24] S. Tang, Y. Liang, Y. Peng, Y. Hu, Y. Liao, X. Yang, H. Zhang, Y. Lin, K. Zhang, J. Liang, B. Li, G. Zhao, Y. Wei, Z. Gong, Y. Yang, Adv. Energy Mater. 2024, 15, 2402842.
- [25] Y. Lu, C.-Z. Zhao, J.-Q. Huang, Q. Zhang, Joule 2022, 6, 1172.
- [26] E. S. Ilton, J. E. Post, P. J. Heaney, F. T. Ling, S. N. Kerisit, Appl. Surf. Sci. 2016, 366, 475.
- [27] Z. W. Yin, W. Zhao, J. Li, X. X. Peng, C. Lin, M. Zhang, Z. Zeng, H. G. Liao, H. Chen, H. Lin, F. Pan, Adv. Funct. Mater. 2021, 32, 2107190.
- [28] R. Sim, L. Su, A. Dolocan, A. Manthiram, Adv. Mater. 2023, 36, 2311573.
- [29] H. Ota, Y. Sakata, A. Inoue, S. Yamaguchi, J. Electrochem. Soc. 2004, 151, A1659.
- [30] X. Teng, C. Zhan, Y. Bai, L. Ma, Q. Liu, C. Wu, F. Wu, Y. Yang, J. Lu, K. Amine, ACS Appl. Mater. Interfaces 2015, 7, 22751.
- [31] G. G. P. Ribière, D. Mathiron, S. Grugeon, M. Armand, J.-B. Leriche, S. Pilard, S. p. Laruelle, Anal. Chem. 2011, 83, 478.
- [32] M. Metzger, B. Strehle, S. Solchenbach, H. A. Gasteiger, J. Electrochem. Soc. 2016, 163, A798.
- [33] T. Liu, L. Lin, X. Bi, L. Tian, K. Yang, J. Liu, M. Li, Z. Chen, J. Lu, K. Amine, K. Xu, F. Pan, Nat. Nanotechnol. 2019, 14, 50.
- [34] J. Wandt, A. Freiberg, R. Thomas, Y. Gorlin, A. Siebel, R. Jung, H. A. Gasteiger, M. Tromp, J. Mater. Chem. A 2016, 4, 18300.
- [35] S. Solchenbach, G. Hong, A. T. S. Freiberg, R. Jung, H. A. Gasteiger, J. Electrochem. Soc. 2018, 165, A3304.